Effect of pressure on $La_2(WO_4)_3$ with a modulated scheelite-type structure

N. P. Sabalisck,[1] J. López-Solano,[2,3,*] C. Guzmán-Afonso,[4] D. Santamaría-Pérez,[5,6] C. González-Silgo,[2] A. Mujica,[2] A. Muñoz,[2] P. Rodríguez-Hernández,[2] S. Radescu,[2] X. Vendrell,[7] L. Mestres,[7] J. A. Sans,[6,8] and F. J. Manjón[8]

[1]*Departamento de Física Básica, Universidad de La Laguna, 38206 Tenerife, Spain*

[2]*Departamento de Física Fundamental II, MALTA Consolider Team, and Instituto de Materiales y Nanotecnología, Universidad de La Laguna, 38206 Tenerife, Spain*

[3]*Izaña Atmospheric Research Center, Agencia Estatal de Meteorología (AEMET), 38071 Tenerife, Spain*

[4]*Departamento de Física Fundamental y Experimental, Electrónica y Sistemas, Universidad de La Laguna, 38206 Tenerife Spain*

[5]*Departamento de Química Física I, and MALTA Consolider Team, Universidad Complutense de Madrid, 28040 Madrid, Spain*

[6]*Departamento de Física Aplicada-ICMUV, and MALTA Consolider Team, Universidad de Valencia, Edificio de Investigación, 46100 Burjassot, Spain*

[7]*Grup de Química de l'Estat Sòlid, Departament de Química Inorgànica, Universitat de Barcelona, 08028 Barcelona, Spain*

[8]*Instituto de Diseño para la Fabricación y Producción Automatizada, and MALTA Consolider Team, Universitat Politècnica de València, 46022 València, Spain*

(Received 1 June 2013; revised manuscript received 8 March 2014; published 27 May 2014)

We have studied the effect of pressure on the structural and vibrational properties of lanthanum tritungstate $La_2(WO_4)_3$. This compound crystallizes under ambient conditions in the modulated scheelite-type structure known as the α phase. We have performed x-ray diffraction and Raman scattering measurements up to a pressure of 20 GPa, as well as *ab initio* calculations within the framework of the density functional theory. Up to 5 GPa, the three methods provide a similar picture of the evolution under pressure of α-$La_2(WO_4)_3$. At 5 GPa, we begin to observe some structural changes, and above 6 GPa we find that the x-ray patterns cannot be indexed as a single phase. However, we find that a mixture of two phases with $C2/c$ symmetry accounts for all diffraction peaks. Our *ab initio* study confirms the existence of several $C2/c$ structures, which are very close in energy in this compression range. According to our measurements, a state with medium-range order appears at pressures above 9 and 11 GPa, from x-ray diffraction and Raman experiments, respectively. Based upon our theoretical calculations we propose several high-pressure candidates with high cationic coordinations at these pressures. The compound evolves into a partially amorphous phase at pressures above 20 GPa.

DOI: 10.1103/PhysRevB.89.174112 PACS number(s): 62.50.−p, 61.05.cp, 78.30.−j, 71.15.Nc

I. INTRODUCTION

Lanthanum tritungstate belongs to the $A_2(BO_4)_3$ family of compounds, a large group which includes materials with optical, ferroelastic, and ferroelectric properties, which make them useful in diverse technological fields [1]. Under normal conditions, the rare-earth (RE) tritungstates and trimolybdates $RE_2(MO_4)_3$ (M = W, Mo) adopt different crystalline structures depending on both the RE cation as well as the method used during the synthesis. Light rare-earth compounds $RE_2(MO_4)_3$ (with RE = La–Dy and M = Mo or W) crystallize in several structures related to the scheelite-type structure of $CaWO_4$ through vacancy ordering of one third of the calcium positions [2]. The trimolybdates of La, Ce, Pr, and Nd adopt a monoclinic structure with space group (SG) $C2/c$, No. 15, and $Z = 12$ formula units per conventional cell [3]. Nd, Sm, Eu, Gd, and Tb trimolybdates and La–Dy tritungstates crystallize in the so-called α-phase (Fig. 1), a crystal structure with SG $C2/c$ and $Z = 4$. Other structures with SG $P2_1/c$, No. 14, and $Z = 4$ are found in related compounds like $Bi_2(MoO_4)_3$, $Sb_2(SO_4)_3$, and $As_2(SO_4)_3$ [1]. Trimolybdates and tritungstates with heavier RE cations (RE = Ho–Lu) adopt the γ form of $Sc_2(WO_4)_3$ and display negative thermal expansion (NTE) [4–6]. A metastable ferroelectric phase with the β' form of $Gd_2(MoO_4)_3$ appears for intermediate molybdates with RE = Nd–Dy [4], but this has never been observed in tritungstates.

The denser α-phases of the Nd, Tb, and Eu trimolybdates undergo pressure-induced amorphization (PIA) at pressures between 15 and 20 GPa. Raman studies show that this process is partially reversible, and it has been suggested that it is related to the random orientation of the MoO_4 tetrahedra [7]. The PIA undergone by ferroelectric trimolybdates with the β'-$Gd_2(MoO_4)_3$ structure has been more extensively studied and is substantially different, with an irreversible amorphization taking place at ∼4 GPa [8]. The amorphization mechanism of both the α and β' phases of $Eu_2(MoO_4)_3$ has been described in a recent study using x-ray absorption spectroscopy (XAS), Raman spectroscopy, and first-principles calculations [9,10]. As pressure increases, a self-reorganization of the oxygen atoms around the Mo and Eu subnetworks develops, inducing a change in the coordination number of the Mo atoms. The authors of these works emphasize the study of the β' phase, which has also been dealt with in previous photoluminescence and Raman spectroscopy studies.

The α phases of trimolybdates have been less studied than the β' or γ phases, as evidenced in a recent review by Maczca *et al.* on pressure-induced phase transitions and amorphization in the tungstate and molybdate families [1]. In fact, the α phases of tritungstates $RE_2(WO_4)_3$ (RE = La–Dy) have never been investigated under compression. In this work, we present the results of a high-pressure experimental and theoretical study on the structural and vibrational properties

*Corresponding author: javierl@marengo.dfis.ull.es

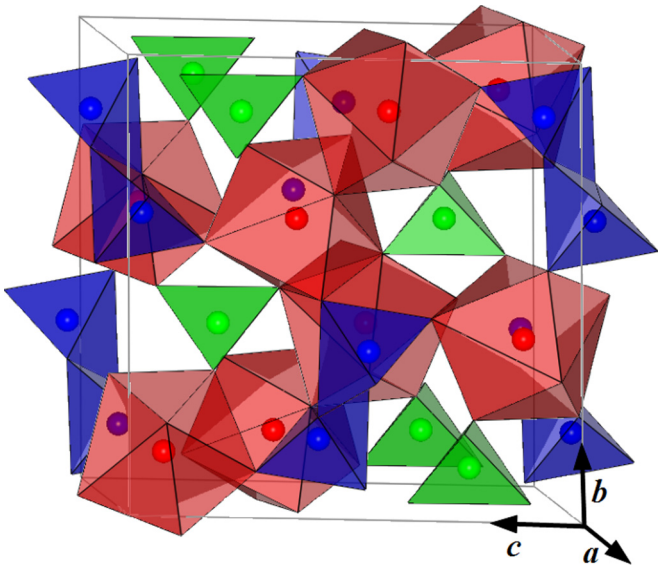

FIG. 1. (Color online) The α phase of $La_2(WO_4)_3$. This structure features two different W environments: the W(1) cations (shown in green) form isolated tetrahedra near the La vacancies and two nearby W(2) cations (blue) create W_2O_8 units. Lanthanum cations (in red) are eightfold coordinated [2].

of $La_2(WO_4)_3$. We analyze its long-range structure and molecular-scale interactions, by means of a combination of x-ray diffraction and Raman spectroscopy measurements, respectively. Furthermore, *ab initio* theoretical calculations are used to complement our experimental results, providing in particular details on phase stability. In this way, we obtain a comprehensive and coherent picture of the complex behavior of $La_2(WO_4)_3$ under pressure.

II. METHOD

A. Experimental

1. Synthesis

$La_2(WO_4)_3$ was prepared by the conventional solid-state ceramic method. High purity chemicals La_2O_3 (Fluka, 99%) and H_2WO_4 (Aldrich, 99%) were used as raw materials. Oxides were treated at 1173 K for 8 hours. The powders were weighed in stoichiometric amounts, mixed, and homogenized in an agata mortar. The resulting powder was then pressed into pellets by applying 100 MPa of uniaxial pressure. Pellets were thermally treated twice for 7 hours at 1273 K. Compacts were homogenized again in an agata mortar. Samples were sintered at 1273 K for 15 hours under air atmosphere. In order to check the purity of the sample, x-ray patterns were measured at room conditions by continuous scanning with a step of 1°/min, using a PANalytical XPert PRO diffractometer (Bragg-Brentano mode) with a primary monochromator of Ge (111) and an XCelerator detector, using Cu $K_{\alpha 1}$ radiation (40 kV and 30 mA) in the angular range $10^\circ < 2\theta < 80^\circ$.

2. X-ray diffraction under pressure

Angle-dispersive x-ray diffraction measurements were carried out with an Xcalibur diffractometer. X-ray diffraction patterns were obtained on a 135-mm Atlas CCD detector placed at 110 mm from the sample using $K_{\alpha 1}$: $K_{\alpha 2}$ molybdenum radiation. The x-ray beam was collimated to a diameter of 300 μm. The observed intensities were integrated as a function of 2θ in order to give conventional one-dimensional diffraction profiles. High-pressure measurements on $La_2(WO_4)_3$ powder were performed in a modified Merrill-Bassett diamond anvil cell (DAC) up to a pressure of 18 GPa. Two diamond anvils were used, with culet sizes of 800 and 500 μm, and stainless-steel gaskets featuring 400-μm- and 150-μm-diameter holes, respectively, and a thickness of 50 μm. The white $La_2(WO_4)_3$ powder sample was placed inside the holes within a 4 : 1 mixture of methanol/ethanol, which was used as pressure-transmitting medium. Ruby chips evenly distributed in the pressure chamber were used to measure the pressure by the standard ruby fluorescence method. Exposure times were typically of 1 hour. The diamond cells used for these experiments allowed access to an angular range $4\theta = 50^\circ$. The CrysAlis software (version 171.34.49, Oxford Diffraction Limited) was used for the collection and preliminary reduction of the data. This experimental setup has been previously used to successfully characterize the high-pressure phases of other oxides in the same pressure range [11].

Two experiments were performed in the aforementioned conditions. In the first experiment, the diffractograms were collected at room conditions under increasing compression at pressures of 1.4, 2.6, 3.8, 5.0, 6.0, 6.4, 7.3, 8.4, 11.4, 13.7, 15.3, and 17.8 GPa, and then at 9.2, 4.8, and 0.1 GPa during decompression. In the second experiment, the diffractograms were measured under compression from room pressure up to 7.4 GPa at 1.2 GPa steps, and at 3.1 and 0.2 GPa during decompression.

The indexing and Rietveld refinement of the powder patterns were performed using the POWDERCELL [12] and FULLPROF [13] software packages. We started from the crystallographic cell of $La_2(WO_4)_3$ (SG $C2/c$, No. 15) [3], an instrumental resolution function (Thomson-Cox-Hastings pseudo-Voight with axial divergence asymmetry), and the background modeled by a Chebyshev polynomial with four coefficients. The initial profile parameters U, V, W, X, and Y as well as the asymmetry parameters were refined using the diffractogram at room pressure with fixed atomic coordinates. From the diffractograms of the two experiments, we obtained the scale factors, the cell parameters, the microstrain (given by U, the other parameters being fixed), and the background coefficients.

3. Raman spectroscopy

Raman scattering experiments up to 20 GPa at room temperature were performed using a HORIBA Jobin Yvon LabRAM HR UV spectrometer in combination with a thermoelectrically cooled multichannel CCD detector with a resolution below 2 cm^{-1}. Excitation was done with a 10 mW, 633-nm HeNe laser focused by a 50× large-working-distance objective. $La_2(WO_4)_3$ powder samples were placed in a membrane-type DAC to carry out the high-pressure Raman measurements. A mixture of methanol-ethanol water (16 : 3 : 1) was used in this case as pressure-transmitting medium [14] and the pressure was measured using the ruby fluorescence technique, similarly

to the x-ray experiments. The background of the experimental Raman spectra was subtracted and vibration modes were analyzed by fitting the Raman peaks with a Voigt profile.

B. Theoretical

Our theoretical calculations were performed within the *ab initio* framework of the density functional theory, using the plane-waves pseudopotential method as implemented in the VASP code [16,17]. We used projector-augmented wave pseudopotentials [18,19] and the PBEsol prescription for the exchange and correlation energy within the generalized gradient approximation [20]. The $5s^2$, $5p^6$, $6d^1$, and $6s^2$ electrons of La, the $5p^6$, $5d^4$, and $6s^2$ of W, and the $2s^2$ and $2p^4$ of O were allowed to relax in the calculations, with the remaining electrons being kept frozen at the atomic cores. To ensure a total-energy convergence of 1 meV per formula unit, we used plane-wave basis sets with an energy cutoff of 520 eV and dense Monkhorst-Pack grids [21] appropriate for each structure considered—for example, a $4 \times 4 \times 2$ grid (resulting in 20 independent **k** points) was used for the ambient-conditions α phase with two formula units in the primitive unit cell, and a $3 \times 2 \times 2$ grid (eight **k** points) was used for the $Bi_2(MoO_4)_3$-type structure with four formula units in the unit cell. For each structure and volume considered, a full optimization of the atomic positions and lattice parameters was performed, constrained to the symmetry compatible with the initial space group and set of Wyckoff positions. In the final optimized configurations, atomic forces were required to be smaller than 0.005 eV/Å^3, and the stress tensor to be diagonal with differences between its components of less than 0.1 GPa.

In our theoretical study of the stability of the α phase, we considered several structures as potential high-pressure candidates, some already known from previous works in related compounds and others found by *ab initio* random structure searching (AIRSS) using our own computational tools. In the latter case, we considered two different methods to generate random structures, both of which have been applied successfully to the search of high-pressure stable phases in other systems (see Ref. [22] and references therein). In the first method, we started from the experimentally determined crystal structure of the α phase and applied random displacements to a random number of randomly selected atoms. In the second method, we assigned random values to all the free parameters of a crystallographic unit cell with four formula units in the 4e Wyckoff positions of SG $P2_1/c$, which is a very usual configuration for ternary oxides [23]. In both methods, structures with unphysically small interatomic distances below 1 Å were discarded. We also calculated the valence of the atoms in the randomly generated structures using the bond valence method [24] and rejected those structures in which the calculated valence of any atom presented a large deviation from the ideal value. All these constrains (symmetry, distances, and valences) ensured that the randomly generated structures had at least some of the features expected for a stable phase and thus made our random search more efficient. The structures obtained in this way were fully optimized at constant volume, in a multiple-step procedure which started with a low-precision calculation (low energy cutoff and **k**-point sampling) and ended with an accurate calculation with the parameters already described at the beginning of this section. Full energy-volume curves were calculated for the most competitive structures according to their energy and pressure values.

We also performed phonon calculations for the most promising candidate structures using the direct force constant (or supercell) method [25,26]. This allowed us to obtain the polarization vectors and frequencies of the Raman and infrared active modes at the Γ zone center. Zero-point motion and temperature effects were not included in the calculations, however.

III. RESULTS AND DISCUSSION

A. Pressure evolution of diffraction patterns

Up to a pressure of 6 GPa, we did not observe any substantial change in the x-ray diffraction patterns (Fig. 2). The x-ray patterns evolved smoothly with increased compression, displaying the characteristic peak broadening observed in other scheelite tungstates [2]. In this range of pressures, all diffractograms could be fitted with the monoclinic α phase. This is shown in Fig. 3 for the patterns collected at 3.8 and 6 GPa during our first experiment. As shown in both Figs. 2 and 3, a sudden splitting into several peaks started at 3.8 GPa, but the diffraction patterns still could be indexed in SG $C2/c$, indicating just a small cell deformation. As we will discuss later, this may indicate some kind of pretransitional effect. The obtained Rietveld refinements were of good quality. At room conditions, the estimated R factors were $R_{wp} = 2.96\%$ and $R_B = 2.90\%$. In Table I, we show the structural data of the ambient-pressure α phase.

The diffraction pattern at 6.4 GPa measured during our first experiment showed several changes (Fig. 3). The peak splitting was lost, new weak diffraction peaks appeared between 12° and 14°, and suddenly the diffraction peaks were shifted towards higher angles. This was accompanied by an increased peak

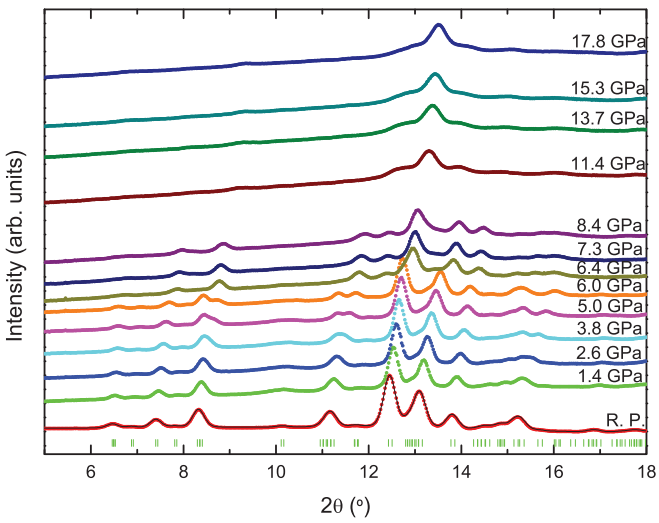

FIG. 2. (Color online) X-ray diffraction patterns of $La_2(WO_4)_3$ from ambient pressure (R.P.) up to 17.8 GPa. The fitted profile for ambient pressure is also shown (dotted line: observed intensities; solid line: profile fit).

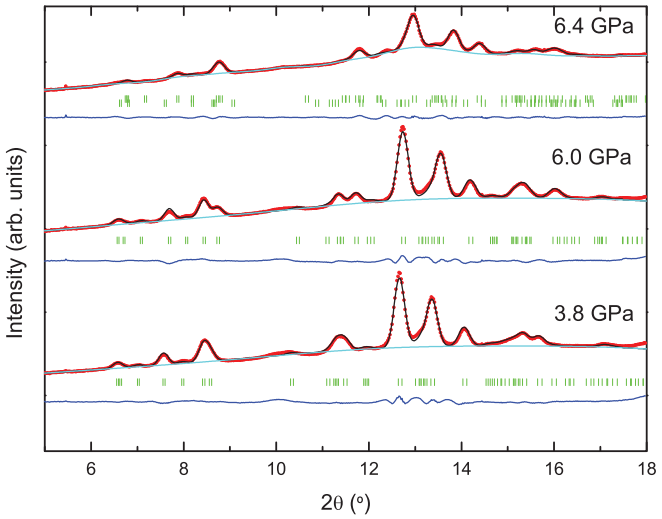

FIG. 3. (Color online) Fitted profile and difference plots for different pressures: during the pre-transition at 3.8 GPa, just before the first phase transition at 6 GPa and after the first phase transition at 6.4 GPa, where we find two phases mixed up. The dotted line indicates the observed intensities, and the profile fit is shown by the solid line. The difference between observed and calculated intensities is plotted at the bottom, and the vertical bars represent the expected positions of diffraction peaks. The smooth light blue curve is the calculated background.

broadening and a loss of diffraction signal. Similar patterns continued to exist up to 8.4 GPa. This is indicative of a first phase transition starting at ∼6 GPa from the ambient-conditions α-phase towards a phase with a different symmetry which would be stable up to 8.4 GPa at least. Diffractograms measured between 6.4 and 8.4 GPa were tentatively indexed with the α phase but at least two peaks were not successfully fitted. We tried other monoclinic subgroups like $P2_1/c$, $P2/c$, Cc, and $C2$, with the initial structure slightly distorted, but the results were also not satisfactory.

Following the indications of our theoretical calculations, which suggest a coexistence of phases (see Sec. III D), we then performed a Rietveld analysis with a mixture of phases. In this refinement, two phases with SG $C2/c$ but with very different lattice and atomic coordinates were used. Henceforth, we will refer to these two phases as α_1 and α_2. The reliability factors at 6.4 GPa were $R_{wp} = 1.03\%$, with $R_{B,1} = 3.64\%$ for the α_1 phase and $R_{B,2} = 9.19\%$ for the α_2. The corresponding values at 7.3 (8.4) GPa were $R_{wp} = 0.899\%(0.804\%)$, $R_{B,1} = 3.68\%(2.89\%)$, and $R_{B,2} = 10.8\%(6.23\%)$. The α_1 phase is similar to the ambient-conditions α phase, while the α_2 implies a considerable structural rearrangement. As a final remark with regard to this first phase transition beyond 6 GPa, we note that the signal/background deterioration and the increased line broadening in this range of pressures cannot be explained by the loss of hydrostaticity of the transmitting medium. These changes may be related to some kind of atomic positional disorder, so that other phases with similar structures might be also present in this mixture. We have observed a similar behavior in other RE tungstates, which also adopt the α phase [27].

Moreover, the changes observed in the diffraction profiles up to 7.4 GPa during the second experiment were found to be reversible, as it is shown in the patterns at 3.1 GPa and 0.2 GPa obtained during descompression in this second experiment (Fig. 4). In particular, note that the diffractogram measured at 3.1 GPa during decompression in the second experiment matches the one measured at 1.9 GPa while increasing pressure in the first experiment. This result indicates a hysteresis in the compression-decompression cycle, compatible with the existence of different phases differing only slightly in their enthalpies as found in the theoretical calculations, see Sec. III D. After releasing the pressure, any component of the mixture of phases observed after the first phase transition may be recovered.

Although at 11.4 GPa (Fig. 2) the action of deviatoric stresses associated with nonhydrostatic conditions within the pressure chamber may affect the quality of the diffraction patterns, deteriorating the signal to background ratio, and producing line broadening [15], the observed changes in the line profile suggest nonetheless that a new phase transition has taken place between 8.4 and 11.4 GPa. This view is

TABLE I. Structural data of the α phase at ambient pressure, as determined by our x-ray diffraction measurements and *ab initio* calculations. Volume is given per two formula units.

	X-ray diffraction measurements	*Ab initio* calculations
V (Å^3)	511.6(4)	513
a (Å)	7.871(3)	7.910
b (Å)	11.828(5)	11.789
c (Å)	11.643(6)	11.670
β (deg.)	109.28(7)	109.468
La (8f)	(0.3200(2), 0.3737(1), 0.4041(1))	(0.3198, 0.3735, 0.4050)
W1 (8f)	(0.1531(2), 0.3538(1), 0.0460(1))	(0.1526, 0.3538, 0.0455)
W2 (4e)	(0.5, 0.6185(1), 0.25)	(0.5, 0.6181, 0.25)
O1 (8f)	(0.6205(23), 0.2891(19), 0.4246(13))	(0.6164, 0.2883, 0.4293)
O2 (8f)	(0.0688(27), 0.3009(18), 0.4639(15))	(0.0722, 0.3011, 0.4626)
O3 (8f)	(0.2175(27), 0.4240(17), 0.1879(16))	(0.2231, 0.4219, 0.1918)
O4 (8f)	(0.1851(26), 0.2037(18), 0.2787(15))	(0.1919, 0.2058, 0.2802)
O5 (8f)	(0.1392(26), 0.5409(19), 0.4393(15))	(0.1357, 0.5365, 0.4398)
O6 (8f)	(0.5132(23), 0.5404(16), 0.3856(15))	(0.5127, 0.5401, 0.3872)

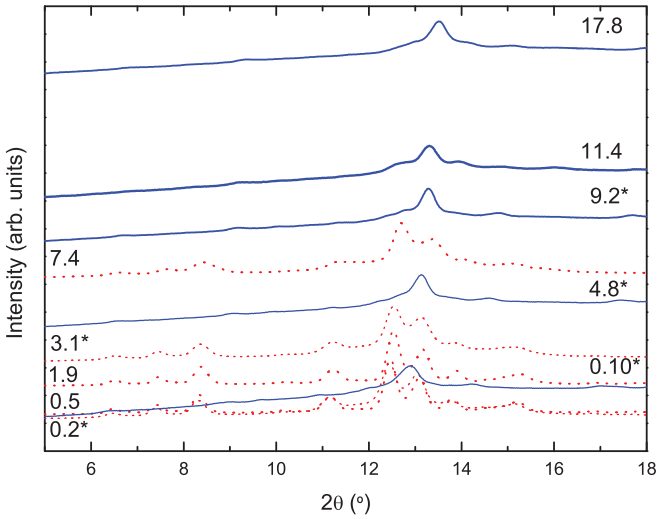

FIG. 4. (Color online) Selected x-ray diffraction patterns of $La_2(WO_4)_3$ for the first (blue) and the second (red) experiments. The pressures of the first (second) experiment are shown on the right (left) side of the patterns. Pressures measured during decompression are marked with an star.

supported by the fact that similar patterns persist up to the maximum experimental pressure reached of 17.8 GPa. This second phase transition would take place at ∼9–10 GPa in agreement with our Raman and theoretical results discussed in following sections, as well as with our own measurements performed in other RE tritungstates [27]. Even though the measured high-pressure diffractograms were inadequate for Rietveld refinement, the new phase seems disordered and without long-range three dimensional order, but not completely amorphous. Henceforth, we will refer to this structure as the "preamorphous phase."

During the pressure release from 17.8 GPa in the first experiment, the pre-amorphous phase presented similar line shapes to those measured at ∼11.4 GPa, showing an irreversible degradation of the diffraction signal. The phases in the range from 6.4 to 8.4 GPa, and between 0 and 6 GPa were not recovered in decompression from 17.8 GPa, in agreement with our Raman measurements. The aforementioned signal/background ratio, which must have deteriorated from 9–10 GPa, was preserved too. However, when pressure is completely released, the broad peaks of the pre-amorphous phase shift to lower angles, indicating some structural relaxation (Fig. 4).

Although the α phase of tritungstates and trimolybdates is quite dense (more than, for example, their β'-phase counterparts [1]), it is also very inhomogeneous, with stoichiometric vacancies that allow rotations and deformations of the tetrahedra, as well as changes in the oxygen polyhedra surrounding the trivalent metal. Reversible phase transitions at lower pressures may be thus the result of rotations of the WO polyhedra around the W cations, leading to one or more O atoms, not belonging to the initial WO_4 tetrahedron, to come close enough to the W atom so as to increase its coordination number to five or more. At higher pressures, steric hindrance between polyhedra is believed to be the most relevant mechanism for amorphization [8,9], and thus the formation of polyhedral units may lead to a loss of long-range order. However, the irreversibility of this process is not explained, in contrast with the reversibility of the successive structural phase transitions at lower pressure. The short or medium range order, which is maintained over a wide range of pressures (probably from 9–10 to 20 GPa) and the irreversibility of the second transition could be related to the formation of stacking faults. This process has been suggested in the case of the incommensurate structure of $Pr_2(MoO_4)_3$, where the coexistence of different rearrangements of the vacancies is possible [28]. A completely amorphous phase could be thus explained as an assemblage of a large number of structures with stacking faults generated through an irreversible mechanism [29].

B. Experimental pressure dependence of the cell parameters

In this section we discuss the effect of compression on the lattice parameters of $La_2(WO_4)_3$, and compare it with the effect of the chemical pressure produced by changes of the ionic radius of the RE element. In Fig. 5, we represent the evolution of the lattice parameters as a function of both pressure and ionic radius, in the latter case showing data for the $RE_2(WO_4)_3$ (RE = La, Ce, Pr, Nd, Eu, Gd, Dy) compounds as found in the ICSD database [30] and Shannon's compilation of ionic radii [31].

The observed smooth variation of the lattice parameters indicates that $La_2(WO_4)_3$ does not undergo any phase transition up to 6 GPa. The variation of all experimental lattice constants with pressure is almost isotropic, showing a monotonic contraction when pressure increases, in agreement with the shift of the x-ray diffraction peaks to higher 2θ angles and of the Raman peaks to higher frequencies (see Sec. III C). The observed splitting into several peaks above 3.8 GPa is correlated with the slight change in the slope of all the cell parameters above this pressure. This may suggest a pretransitional effect in accordance with the theoretical calculations, after which the b and c lattice parameters contract rather anisotropically, so that the structure becomes more compressible along the c axis. Note also that the a parameter decreases smoothly and the fast decrease of the β angle. A fit using a second-order Birch-Murnaghan equation of state in this range of pressures produces a bulk modulus of $B_0 = 63.4(8)$ GPa, which is similar to the ones reported by Errandonea *et al.* [32] for $PbWO_4$ and $BaWO_4$ before these materials undergo their first phase transition. This similitude could be the result of a major influence of the WO_4 units on the total compressibility.

The α_1 and α_2 structures observed at pressures above 6 GPa present some striking differences with respect to the initial α phase. The pressure dependence of the two cells is different in the three spatial directions. The b and c parameters of the α_1 structure display almost isotropic compressibility, and the c axis remains unchanged through the phase transition. The a axis also decreases while the β angle increases abruptly. In the α_2 structure, the pressure dependence of the b and c parameters is clearly anisotropic, c being softer than b, and their lengths become similar at high pressures. The a axis increases abruptly at the phase transition but under pressure it contracts until it reaches the same length as the a axis of the ambient-conditions α phase. The β angle of the α_2 phase

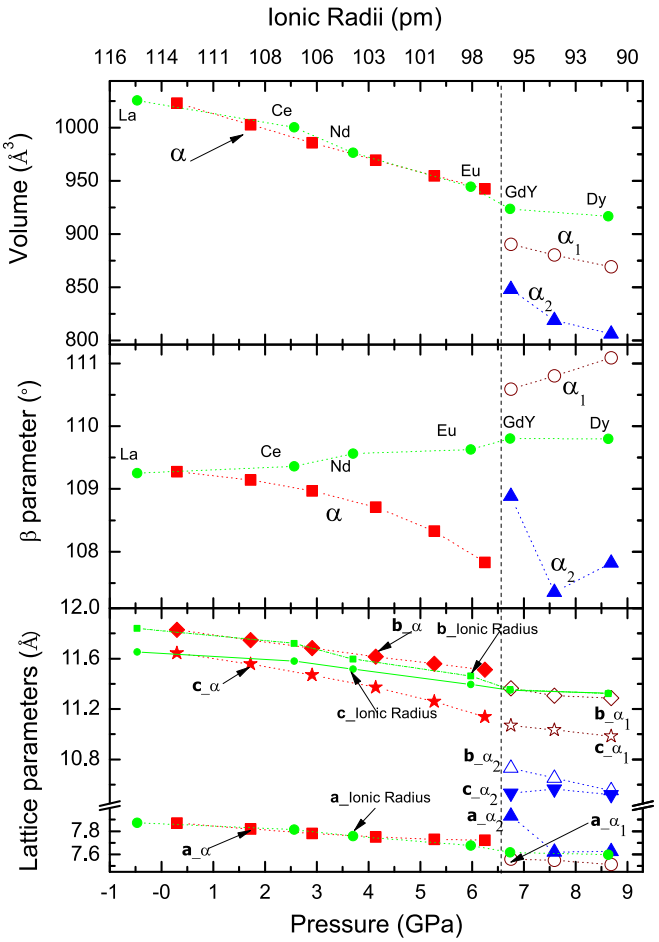

FIG. 5. (Color online) Pressure dependence of the cell volume (top), monoclinic angle (middle), and lattice parameters (bottom) for $La_2(WO_4)_3$, plotted along data for other tritungstates as a function of the ionic radii, extracted from the ICSD database [30] and Shannon's compilation [31]. Error bars at low pressures and for compounds with different ionic radii are smaller than the symbols used in the plots. Vertical dashed lines show the first phase transition pressure, whereas other lines are just a guide for the eye. Green symbols correspond to ionic radii data, red ones to the α phase before transition, and purple and blue ones to the α_1 and α_2 phases after the transition, respectively.

behaves in a way that is similar to that of the a parameter. The bulk moduli of the α_1 and α_2 phases are, respectively, 35.7(6) and 21.6(7) GPa. For comparison, $Sc_2(WO_4)_3$ crystallized in the γ phase undergoes an orthorhombic-to-monoclinic pressure-driven phase transition at 14 GPa in which the bulk modulus changes from 31 to 14 GPa [1].

With regard to the chemical pressure, the compounds with larger ionic radii are found on the left side of Fig. 5, which corresponds to pressures below the first phase transition, and they clearly behave in a different way under pressure than the compounds on the right side (i.e., above the phase transition). The compounds on the left side show a pressure dependence of their a and b axes very similar to that of the α structure below 6 GPa. The ionic dependence of the β angle is very different to that shown by the α phase, and it is also smaller and features a softer increase than the one shown by the monoclinic angle of the high-pressure α_1 phase. For the compounds on the right side, the lengths of the b and c axes are practically the same, and the a axis and β angle remain constant, as it also happens in the α_2 structure at higher pressure. Interestingly, there is a clear change in volume between the left and right sides. A similar behavior is observed in RE trimolybdates with the α phase, as it can be deduced from Brixner *et al.* [33].

Taking into account both the effect of pressure and ionic radius changes, Fig. 5 shows that the volume of the α structure can be contracted along more than one possible path. Moreover, we have also recently observed a quite different pressure dependence of the cell parameters of α-$Eu_2(MoO_4)_3$ [34]. All this may explain the hysteresis observed in the decompression from 7.4 GPa (Fig. 4).

C. Pressure evolution of Raman spectra

According to group theory [35], the monoclinic structure of α-$La_2(WO_4)_3$ at ambient pressure has 102 vibrational modes at the center of the Brillouin zone:

$$\Gamma : 25A_g(R) + 24A_u(\mathrm{IR}) + 26B_g(R) + 24B_u(\mathrm{IR}) + A_u + 2B_u.$$

Since the structure is centrosymmetric, vibrational modes are either Raman (R) or infrared (IR) active. There are 51 Raman-active modes and 48 IR-active modes, plus one A_u and two B_u acoustic modes.

Figure 6(a) shows Raman scattering measurements of $La_2(WO_4)_3$ performed up to 20 GPa. Raman scattering spectra at low pressures show a large number of Raman modes in good agreement with group theoretical estimations for the α phase. A change in the Raman spectrum occurs above 6.5 GPa followed by other changes above 10 and 16 GPa, respectively. However, Raman spectra do not show signs of complete amorphization up to the maximum pressure reached in our experiment, 20 GPa. In the amorphous phase of a tritungstate, all bands would have disappeared and only three broad massifs should be observed, corresponding to the external (or lattice) modes, bending modes, and stretching modes of the WO_x molecular components. In our experiments, the existence of all these bands close to the bending and stretching modes of the original WO_4 groups suggests that, despite severe deformations, the polyhedral nature remains. Despite not having reached amorphization, the anomalies detected during compression in our Raman measurements may explain possible mechanisms for pressure induced amorphization. We will describe these anomalies later.

Figure 6(b) shows the pressure dependence of the experimental Raman modes on upstroke to 20 GPa (full symbols) and downstroke till ambient pressure (empty symbols). Up to 6.5 GPa, most of the Raman peaks of the α phase exhibit a monotonic shift of frequency with pressure which is consistent with the contraction of the unit cell parameters shown by our x-ray diffraction measurements up to 6 GPa. Table II summarizes the experimental and theoretical frequencies and pressure coefficients at ambient pressure for the α phase, showing a good agreement between both methods. Overall, in this range of pressures, the experimental Raman modes are in good agreement with the ones obtained in our *ab initio* calculations (see the supplemental material for full details [36]).

The most clear signature of the α phase is the weak and isolated mode occurring near 541 cm^{-1} at ambient pressure

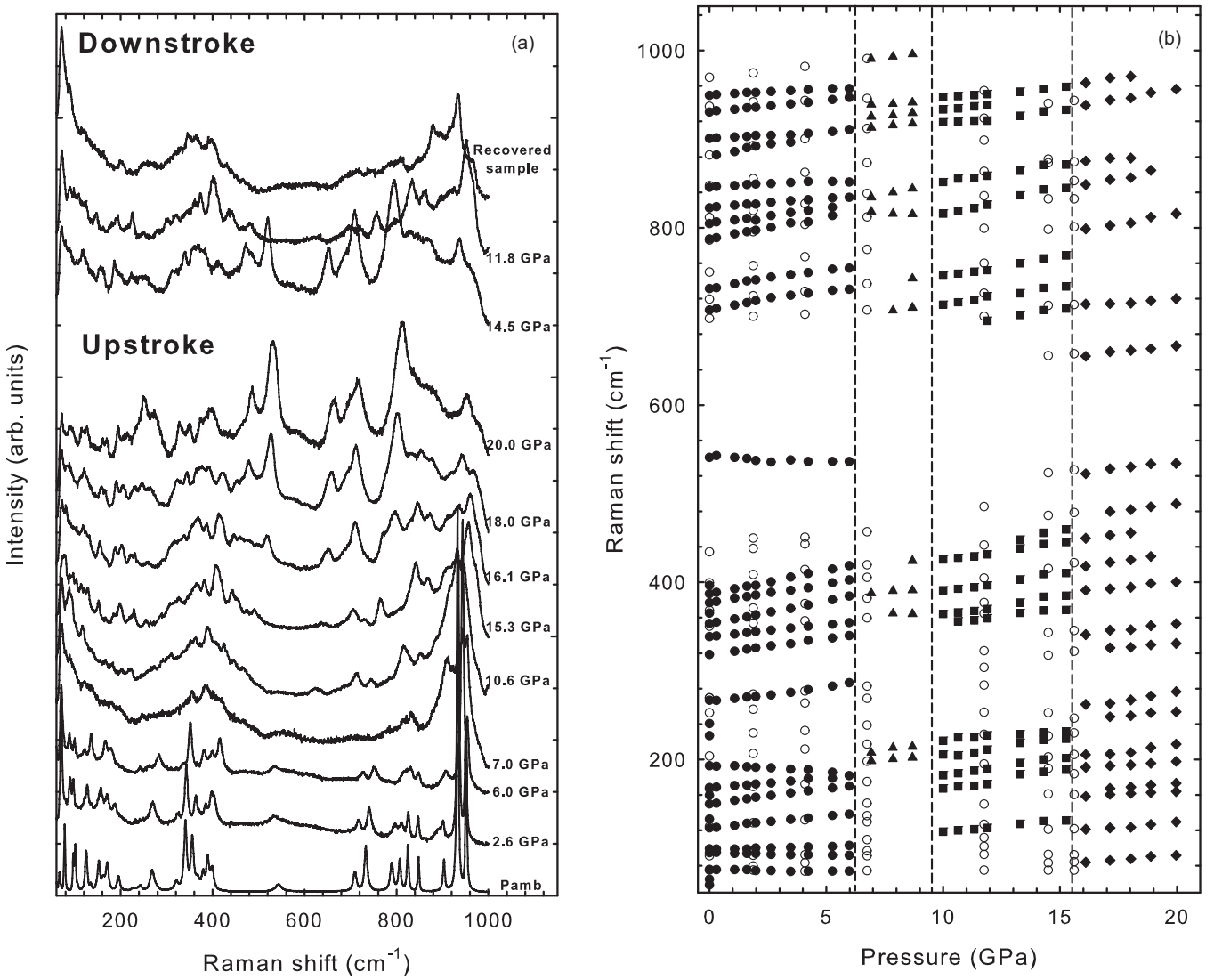

FIG. 6. (a) Raman spectra and (b) Raman modes of $La_2(WO_4)_3$ during compression (filled symbols) from ambient pressure to 20 GPa, and decompression (empty symbols). Phase transitions were observed at 6.5 and 15.1 GPa on compression and at 13.1 GPa on downward stroke. Once the pressure cycle was completed, the sample remained in the second phase.

which is between the bending (below 400 cm^{-1}) and stretching (above 700 cm^{-1}) modes. Besides a softening with increasing pressure, this mode also shows a continuous peak broadening until it becomes undetectable at pressures above 6.5 GPa. The latter characteristic is consistent with the mixture of phases starting at 6–6.5 GPa, as suggested by both our XRD measurements and *ab initio* calculations. This isolated mode could be either the B_g (with a calculated frequency of 541 cm^{-1} at ambient pressure) or the A_g mode (542 cm^{-1} at ambient pressure), or even a combination of both. Note that both modes have a negative pressure coefficient. In particular, we must note that there are three groups of bands with negative pressure coefficient: the lowest-frequency lattice modes; a group of lattice modes between 165 and 190 cm^{-1}; and the group of the highest bending modes near 540 cm^{-1}. We think that this last group could correspond to the highest bending modes of the $C2/c$ structure, because similar bands above 400 cm^{-1} were observed for tungstates of the ABO_4 family with a monoclinic structure [37,38].

Besides the disappearance of the soft mode of 541 cm^{-1} above 6.5 GPa, the three frequency regions corresponding to the original α phase are still present between 6.5 and 10 GPa. However, at pressures above 6.5 GPa, the widths of the Raman peaks are larger. A possible explanation of this feature could be the appearance of new similar modes around the original ones. The complete spectrum seems very smooth, suggesting an increase of positional disorder without a significant change of the structure. X-ray results support the possibility of a mixture of phases, very similar to the original α phase, but with cell parameters that could evolve differently during compression. If the positional disorder was larger, resulting in a lowering of symmetry or in cell multiplicity, new Raman peaks would arise in a less uniform way, so the suggested mixture of phases appears as another plausible explanation. In addition, the stability range of such mixture of phases would be rather narrow, a feature observed both in the x-ray diffraction and Raman experiments, in which new changes are measured above 10 GPa.

TABLE II. Experimental and *ab initio* frequencies (ω_0, in cm^{-1}) and pressure coefficients ($d\omega_0/dP$, in cm^{-1}/GPa) of the Raman-active modes of α-$La_2(WO_4)_3$ at ambient pressure.

	Experimental		*Ab initio*	
Mode symmetry	ω_0	$d\omega_0/dP$	ω_0	$d\omega_0/dP$
B_g	58(1)	–	56	1.87
A_g	65(1)	–	67	−0.92
B_g			68	1.42
A_g	76(1)	−0.36(9)	73	−0.9
B_g	95(1)	−0.59(7)	94	−0.79
A_g	98(1)	0.69(6)	98	0.74
B_g			102	2.6
A_g			119	1.54
A_g	123(1)	2.59(6)	123	1.71
B_g			123	−1.43
B_g	133(2)	–	128	2.26
A_g	150(1)	3.36(6)	144	3.63
B_g	150(1)	3.36(6)	145	2.1
B_g	160(1)	–	155	2.38
A_g	160(1)	–	159	2.00
A_g	168(1)	2.24(8)	165	0.28
B_g			168	0.05
A_g	194(2)	−1.39(9)	185	−1.55
B_g			189	4.87
B_g			200	−1.59
A_g	227(2)	–	222	4.69
B_g	227(2)	–	228	5.7
B_g	240(2)	–	235	4.29
A_g	240(2)	–	236	4.52
A_g			253	2.13
B_g	265(2)	3.44(8)	265	4.97
A_g			305	3.68
B_g			318	5.33
A_g	319(1)	3.56(9)	325	2.61
B_g			328	2.05
A_g	339(1)	2.64(5)	339	4.97
B_g	353(1)	5.16(7)	349	4.68
A_g	365(1)	–	361	4.18
B_g	377(1)	4.17(8)	372	5.4
A_g			372	5.94
B_g	387(1)	5.35(9)	374	5.95
A_g	396(2)	–	376	4.24
B_g	541(2)	−1.0(3)	540	−4.29
A_g	541(2)	−1.0(3)	541	−4.12
B_g	709(1)	3.80(2)	693	4.95
A_g	709(1)	3.80(2)	694	5.14
A_g	732(1)	3.80(2)	721	4.86
B_g	732(1)	3.80(2)	734	4.77
B_g	788(1)	4.85(9)	782	5.00
A_g	805(2)	3.50(3)	800	3.20
A_g	823(1)	1.93(7)	813	1.91
B_g	846(1)	0.96(8)	839	0.95
B_g	882(1)	4.70(5)	894	−0.3
B_g	901(1)	1.53(9)	921	2.66
A_g	931(2)	2.61(6)	924	3.04
A_g	950(2)	1.23(7)	942	−0.46

Between 10 and 15.7 GPa, slight and gradual changes were observed in the Raman spectra. Several modes in the bending and stretching regions show an intensity reversal. Also, with respect to the previous phase, some modes shift upwards or downwards under compression. In this range of pressures, x-ray diffraction results suggest a possible reordering of vacancies through systematic defects (stacking faults, for instance). However, these changes are not evidenced in the Raman spectra, since neither the external nor internal modes of polyhedra around W atoms seem to be affected by those defects. Major changes, compatible with a gradual increase in the cell multiplicity, should be visible in the lattice mode region, where new small and weak peaks would appear.

Beyond 15.7 GPa, more important changes are observed. The shape of the lattice band at lower frequencies remains very similar after the transition, although some peaks are split under compression at higher pressures. In the three regions, the bending and stretching bands decrease considerably in intensity while new bands appear, increasing their intensity and width until they became predominant. The only explanation for these changes is a structural evolution. These results suggest that some nonbonded oxygen atoms get closer to the WO_4 tetrahedra, resulting in an effective increase of the W-O coordination. Therefore new external and internal WO_x modes are possible and the tetrahedral modes weaken, to the point that they even disappear. Note that, because the oxygen sublattice is the principal responsible of these changes, x-ray diffractograms are not sensible to them [1].

On decompression from 20 GPa, we observe some degree of structural recovery, but the final structure is far from the original crystalline state. A new phase develops through some kind of structural relaxation, retaining a highly disordered structure which suggests a loss of positional ordering. Apparently, this new phase is similar to the one observed between 10 and 15.7 GPa [see empty symbols in Fig. 6(b)]. This was also observed in our x-ray diffraction experiments. It may be the result of the reversibility of the rotational and deformation disorder of the WO_4 groups, and also of the formation of new polyhedra around the W atoms, while the vacancies and the La cations still remain disordered in the structure. A similar explanation has been given for NTE compounds [29] and it is compatible with the role of the aforementioned stacking faults. We believe that this explanation is more realistic than suggesting that the deformation of the WO_4 tetrahedra is large enough to prevent a full structural recovery on retrieval [8]. In this respect, we must note that nonreversible pressure-induced phase transitions, due to the irreversibility of order-disorder processes, are also common in other compounds containing ordered vacancies at cation sites in the room-pressure phase. In particular, when the pressure-induced phase transition involves a total disorder of cations and vacancies, the original ordered structure cannot be recovered on downstroke. This effect has been observed in recent years in several adamantine-type ordered-vacancy compounds, like for example $CdGa_2Se_4$ [39–41].

D. Compression effects and structural stability from *ab initio* calculations

Figure 7 shows curves of energy as a function of volume for the most stable phases found in our *ab initio* study. They include the structures of the compounds $Eu_2(WO_4)_3$ (which adopts the α phase), $Gd_2(MoO_4)_3$ (with the β' phase at ambient conditions and the β phase at high temperature), $Sc_2(WO_4)_3$

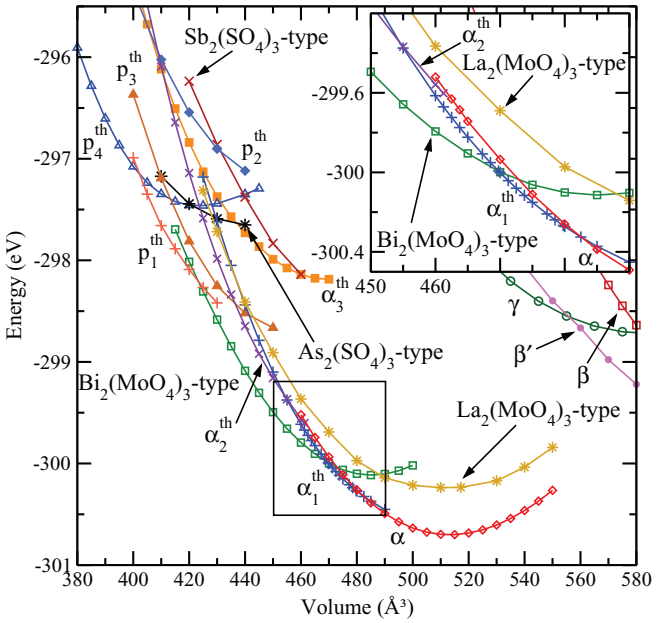

FIG. 7. (Color online) Energy-volume curves for the most competitive structures found in our *ab initio* study, see text for full details. The inset shows the area marked in the main figure. Both energy and volume are given per two formula units.

(with the so-called γ phase), $La_2(MoO_4)_3$, $Bi_2(MoO_4)_3$, $As_2(SO_4)_3$, and $Sb_2(SO_4)_3$. The first six structures are usual ambient-pressure phases of RE molibdates and tungstates, and the α phase, $La_2(MoO_4)_3$ type, and $Bi_2(MoO_4)_3$ type have been described as ordered defect scheelites [3]. In all cases, data found in the ICSD database [30] were used to generate the initial structures, which were then fully optimized.

Besides these already known structures, we have also calculated the energy-volume curves for several other totally novel structures found by AIRSS. We evaluated the energetics of about 200 structures generated by adding random displacements to the structure of the α phase, and found as the most stable ones the structures labeled as α_1^{th}, α_2^{th}, and α_3^{th} in Fig. 7. We also performed a random search on structures with space group $P2_1/c$ and four formula units in 4e Wyckoff positions. Note that the $Bi_2(MoO_4)_3$-type, $As_2(SO_4)_3$-type, and $Sb_2(SO_4)_3$-type structures feature this type of crystallographic unit cell and are quite competitive at high pressures (cf. Fig. 7). Close to 450 structures were fully optimized in this search, and the structures named p_1^{th}, p_2^{th}, p_3^{th} and p_4^{th} turned out to be the most competitive ones among them.

In agreement with our experimental results, the α phase is the most stable structure among those considered in our calculations. The fit of a fourth-order Birch-Murnaghan EOS to a set of energy-volume data of the α phase around the energy minimum provides a value of 513.3 Å^3 for the equilibrium volume per two formula units V_0, 59.2 GPa for the bulk modulus B_0, and 3.6 for the first pressure derivative of the latter B_0'. These values are in good agreement with the experimental data. As shown in Table I, there is also a good agreement between experiments and *ab initio* calculations with regard to the structural parameters of the zero-pressure α structure. Furthermore, Table II shows a good agreement between the calculated and experimental Raman frequencies of the α phase at ambient pressure.

According to our calculations, the α phase is the most stable one among all the phases considered up to a pressure of 3.8 GPa. Between this pressure and up to 7.4 GPa, there is a strong competition in enthalpy among four structures: the original α structure, the α_1^{th} and α_2^{th} structures, and the $Bi_2(MoO_4)_3$-type structure. However, besides taking into account the crossing of enthalpy curves which provide the theoretical coexistence pressures for pressure-driven phase transitions, it is also important to realize that the existence of kinetic barriers does hinder (quite severely in many cases) a massively first-order solid-solid phase transition, which involves large atomic rearrangements. This is the case, for example, of the $BaWO_4$ and $PbWO_4$ ternary oxides, where a barrierless second-order scheelite-to-fergusonite transition takes place instead of the *ab initio* predicted transition from the scheelite-type phase to the $BaWO_4$-II-type ($PbWO_4$-III-type) phase, the latter structure being only observed in x-ray experiments performed at rather higher pressures [37,38,42]. Although the $Bi_2(MoO_4)_3$-type phase is more stable than the α phase at pressures above 3.8 GPa, both structures have a completely different ordering of cations and vacancies [3], and thus the α-to-$Bi_2(MO_4)_3$-type transition should be kinetically hindered and rather unlikely at the predicted coexistence pressure.

As shown in Fig. 8, the lattice parameters of the α_1^{th} and α_2^{th} phases are close to those of the α phase. The difference in enthalpy between these three structures is also quite small, with a maximum difference of ~50 meV per two formula units in the range of pressures between 5 and 8 GPa. The existence of multiple phases with similar crystal structures and enthalpies supports the hypothesis of various coexisting phases between 6 and 9 GPa.

Despite their closeness in energy, the α_1^{th} phase presents marked structural differences with respect to both the α and α_2^{th} phases, and thus a transition from the α phase to the structurally closer α_2^{th} phase is more likely. As per the crossing of their enthalpy-pressure curves, the calculated coexistence pressure is 6 GPa, which is fairly close to the 6.4 GPa value found in our experiments. The calculated structural parameters of the α and α_2^{th} phases at high-pressure are also close to the experimental data of the coexisting phases at high pressure (see Fig. 8). The calculated Raman modes of the α_2^{th} structure are also in qualitative agreement with our experimental measurements (see Ref. [36]). In particular, the frequencies of the lone modes at ~550 cm^{-1} are slightly shifted downwards with respect to their position in the α phase, and those of the bending band are shifted upwards, so that an empty gap develops between 550 and 700 cm^{-1} in the α_2^{th} structure. Note, however, that, if a mixture of phases develops at pressures starting at ~6 GPa, this lone mode could disappear or become indistinguishable from the background, as is indeed observed in our Raman measurements.

As it has been already mentioned, under higher pressure and/or high-temperature conditions, the $Bi_2(MoO_4)_3$-type structure could become stable. Another high-pressure candidate is the p_4^{th} phase, which becomes the most stable phase at ~8 GPa according to the crossing of enthalpy curves. In our experiments, a second phase transition has been observed at 9–10 GPa, but neither the calculated Raman spectra of the

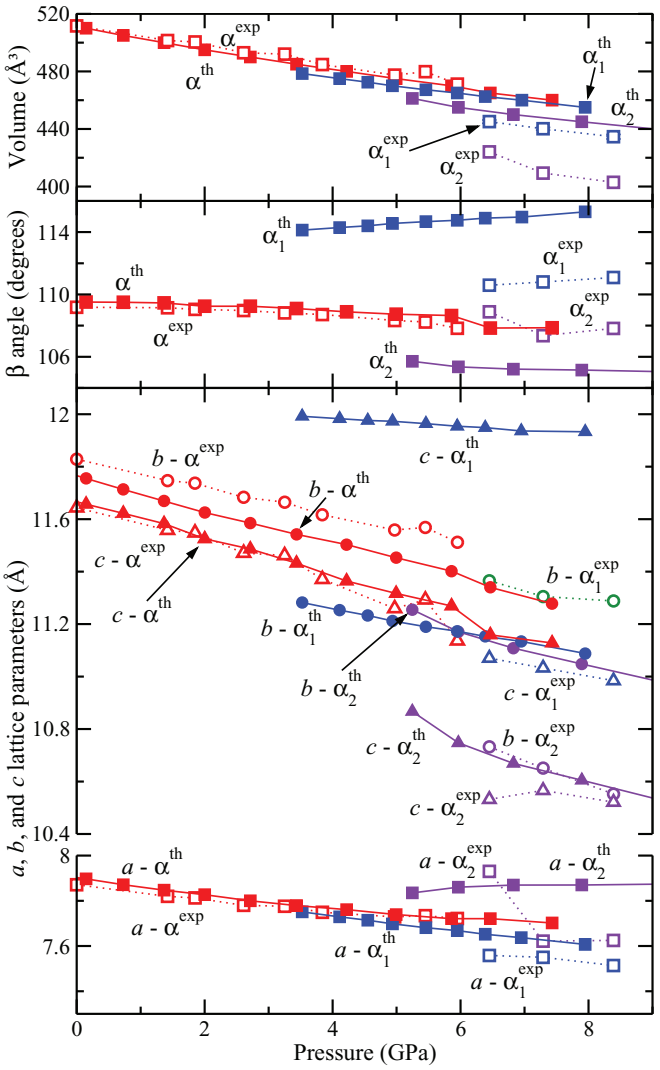

FIG. 8. (Color online) Evolution under pressure of the lattice parameters and volume of the α, α_1 and α_2 structures, according to theory (marked with the *th* superindex and filled symbols) and experiments (*exp* superindex and empty symbols).

$Bi_2(MoO_4)_3$-type structure nor that of the p_4^{th} seem to be in agreement with our measurements in the range from ∼8 to ∼14 GPa. However, the observed increase in the number of modes and in the general broadening of the lattice, bending and stretching bands at pressures above 16 GPa indicate an increase in the cationic coordination which is present in these structures. In the $Bi_2(MoO_4)_3$-type structure, La and W are, respectively, eightfold and sixfold coordinated, whereas in the p_4^{th} structure La is ninefold and W sixfold or eightfold coordinated, depending on the site. It should be noted that these coordinations are also usual for the high pressure phases of the better known ABX_4 compounds [32,43–45].

IV. CONCLUSIONS

We have studied the structural dependence under pressure of the $La_2(WO_4)_3$ tritungstate with modulated-scheelite structure. X-ray diffraction measurements and Raman scattering analysis were performed at room temperature up to maximum pressures of 18 and 20 GPa, respectively. *Ab initio* calculations provided complementary information not available from our experiments.

Up to a pressure of 4 GPa, the behavior of $La_2(WO_4)_3$ does not show any striking change. Our experimental and theoretical results are in good agreement with regard to the values of the EOS parameters at ambient pressure, and also to the evolution of the structural parameters and Raman modes with pressure.

Between 4 and 7 GPa, our theoretical calculations show that other structures become more stable than the α phase. In particular, the α_1^{th} and α_2^{th} are structurally and energetically very close to the α phase. In our x-ray diffraction study, we have indeed been able to refine a mixture of two phases, both with $C2/c$ symmetry, in the interval from 6 GPa up to 9–10 GPa. Further supporting the existence of a mixture of phases, we have experimentally observed a reversibility and hysteresis in the diffraction profiles up to 7.4 GPa, which can be related to the existence of such a mixture. Furthermore, in agreement with the x-ray observations and theoretical calculations, noticeable changes are found in the Raman spectra at pressures above 6.5 GPa. The disappearance of the lone mode located at 550 cm^{-1} could also be related to the formation of a mixture of phases.

Above 9 GPa, we observe a sudden and irreversible loss of crystallinity in our x-ray diffraction measurements, but we have not been able to refine the structure of the new phase (or mixture of phases). This transition is also observed in our Raman spectroscopy measurements. Another important result of our Raman measurements is the large increase of the number of modes at 16 GPa, which is compatible with an increase in the coordination of the W ions. In our theoretical study, we propose several high-pressure candidate structures with different vacancy ordering (as inferred from x-ray diffraction) and large ionic coordinations (as inferred from Raman spectroscopy).

Despite all the modifications observed during compression, a pressure-induced amorphization was not found up to the maximum pressures of 18 and 20 GPa reached in our x-ray diffraction and Raman scattering experiments, respectively. However, the α phase was not recovered upon full pressure release, showing that major atomic rearrangements had taken place. Further experimental and theoretical studies, in this and related materials, would be necessary to completely characterize the pressure induced amorphization process.

ACKNOWLEDGMENTS

We acknowledge the financial support of the Spanish Ministerio de Economía y Competitividad under Grants MAT2010-21270-C04-02/03/04, CTQ2009-14596-C02-01, CSD2007-00045 and the Comunidad de Madrid and European Social Fund S2009/PPQ-1551-4161893. Access to the MALTA Cluster Computer (Universidad de Oviedo), the Atlante Supercomputer (Instituto Tecnológico de Canarias, Red Española de Supercomputación), and the MALTA Xcalibur Diffractometer (Universidad Complutense de Madrid) is gratefully acknowledged. C.G.A. wishes to thank the Agencia Canaria de Investigación, Innovación y Sociedad de la Información, and the European Social Fund of the Gobierno de Canarias for a fellowship. J.A.S. acknowledges financial support through the Juan de la Cierva fellowship program.

[1] M. Maczka, A. G. Souza Filho, W. Paraguassu, P. T. C. Freire, J. Mendes Filho, and J. Hanuza, Prog. Mater. Sci. **57**, 71335 (2012).

[2] K. Boulahya, M. Parras, and J. M. González-Calbet, Z. Anorg. Allg. Chem. **631**, 1988 (2005).

[3] W. Jeitschko, Acta Cryst. B **29**, 2074 (1973).

[4] W. Jeitschko, Acta Cryst. B **28**, 60 (1972).

[5] J. S. O. Evans, T. A. Mary, and A. W. Sleight, J. Solid State Chem **137**, 148 (1998).

[6] C. Guzmán-Afonso, C. González-Silgo, J. González-Platas, M. E. Torres, A. D. Lozano-Gorrín, N. Sabalisck, V. Sánchez-Fajardo, J. Campo, and J. Rodríguez-Carvajal, J. Phys.: Condens. Matter **23**, 325402 (2011).

[7] A. Jayaraman, S. K. Sharma, Z. Wang, and S. Y. Wang, Solid State Commun. **101**, 237 (1997).

[8] G. Lucazeau, O. Le Bacq, A. Pasturel, P. Bouvier, and T. J. Pagnier, J. Raman Spectrosc. **42**, 452 (2011).

[9] O. Le Bacq, D. Machon, D. Testemale, and A. Pasturel, Phys. Rev. B **83**, 214101 (2011).

[10] D. Machon, V. P. Dmitriev, V. V. Sinitsyn, and G. Lucazeau, Phys. Rev. B **70**, 094117 (2004).

[11] E. Bandiello, D. Errandonea, D. Martinez-Garcia, D. Santamaria-Perez, and F. J. Manjón, Phys. Rev. B **85**, 024108 (2012).

[12] W. Kraus and G. Nolze, J. Appl. Crystallogr. **29**, 301 (1996).

[13] J. Rodríguez-Carvajal, Physica B **192**, 55 (1993).

[14] Although concentrations are somewhat different than in our x-ray experiments, different methanol-ethanol-water media behave very much in a similar way under pressure, see Ref. [15].

[15] S. Klotz, J.-C. Chervin, P. Munsch, and G. Le Marchand, J. Phys. D: Appl. Phys. **42**, 075413 (2009).

[16] G. Kresse and J. Hafner, Phys. Rev. B **47**, 558 (1993).

[17] G. Kresse and J. Furthmüller, Phys. Rev. B **54**, 11169 (1996).

[18] G. Kresse and D. Joubert, Phys. Rev. B **59**, 1758 (1999).

[19] P. E. Blochl, Phys. Rev. B **50**, 17953 (1994).

[20] J. P. Perdew, A. Ruzsinszky, G. I. Csonka, O. A. Vydrov, G. E. Scuseria, L. A. Constantin, X. Zhou, and K. Burke, Phys. Rev. Lett. **100**, 136406 (2008).

[21] H. J. Monkhorst and J. D. Pack, Phys. Rev. B **13**, 5188 (1976).

[22] C. J. Pickard and R. J. Needs, J. Phys. Condens. Matter **23**, 053201 (2011).

[23] L. E. Depero and L. Sangaletti, J. Solid Stat. Chem. **129**, 82 (1997).

[24] I. David Brown, *The Chemical Bond in Inorganic Chemistry* (Oxford University Press, New York, 2006).

[25] G. Kresse, J. Furthmüller, and J. Hafner, Europhys. Lett. **32**, 729 (1995).

[26] D. Alfè, Comp. Phys. Comm. **180**, 2622 (2009); program available at http://chianti.geol.ucl.ac.uk/~dario.

[27] N. Sabalisck, L. Mestres, X. Vendrell, E. Cerdeiras, D. Santamaría, V. Lavín, A. Muñoz, P. Rodríguez-Hernández, J. López-Solano, E. Matesanz, and C. Guzmán-Afonso, Acta Cryst. A **67**, C504 (2011)

[28] Logvinovich, A. Arakcheeva, P. Pattison, P. Eliseeva, P. Tomes, I. Marozau, and G. Chapuis, Inorg. Chem. **49**, 1587 (2010).

[29] N. Garg, C. Murli, A. K. Tyagi, and S. M. Sharma, Phys. Rev. B **72**, 064106 (2005).

[30] G. Bergerhoff and I. D. Brown, in *Crystallographic Databases*, edited by F. H. Allen, G. Bergerhoff, and R. Sievers (International Union of Crystallography, Chester, 1987); A. Belsky, M. Hellenbrandt, V. L. Karen, and P. Luksch, Acta Cryst. B **58**, 364 (2002).

[31] R. D. Shannon, Acta Crystallogr., Sect. A: Cryst. Phys., Diffr. Theor. Gen. Crystallogr. **32**, 751 (1976).

[32] D. Errandonea and F. J. Manjón, Prog. Mater. Sci. **53**, 711 (2008).

[33] L. H. Brixner, J. R. Barkley, and W. Jeitschko, *Handbook on the Physics and Chemistry of Rare Earths* (North-Holland Publishing Co., Amsterdam, 1979).

[34] N. Sabalisck, J. González-Platas, V. Lavín, C. Guzmán-Afonso, L. Mestres, and E. Cerdeiras, *Structure, Compression, and Amorphization in Rare Earth Tungstates with Modulated Scheelite-Type Structure under High Pressure*, ALBA Synchrotron experimental report of proposal No. 2012010246, 2012 (unpublished).

[35] E. Kroumova, M. I. Aroyo, J. M. Perez-Mato, A. Kirov, C. Capillas, S. Ivantchev, and H. Wondratschek, Phase Transitions **76**, 155 (2003).

[36] See Supplemental Material at http://link.aps.org/supplemental/10.1103/PhysRevB.89.174112 for further details of the results of the *ab initio* calculations including calculated structural parameters of structures considered at pressures around 8 GPa and evolution of Raman modes.

[37] F. J. Manjón, D. Errandonea, N. Garro, J. Pellicer-Porres, P. Rodríguez-Hernández, S. Radescu, J. López-Solano, A. Mujica, and A. Muñoz, Phys. Rev. B **74**, 144111 (2006).

[38] F. J. Manjón, D. Errandonea, N. Garro, J. Pellicer-Porres, J. López-Solano, P. Rodríguez-Hernández, S. Radescu, A. Mujica, and A. Muñoz, Phys. Rev. B **74**, 144112 (2006).

[39] A. Grzechnik, V. V. Ursaki, K. Syassen, I. Loa, I. M. Tiginyanu, and M. Hanfland, J. Solid State Chem. **160**, 205 (2001).

[40] O. Gomis, R. Vilaplana, F. J. Manjón, E. Pérez-González, J. López-Solano, P. Rodríguez-Hernández, A. Muñoz, D. Errandonea, J. Ruiz-Fuertes, A. Segura, D. Santamaría-Pérez, I. M. Tiginyanu, and V. V. Ursaki, J. Appl. Phys. **111**, 013518 (2012).

[41] O. Gomis, R. Vilaplana, F. J. Manjón, D. Santamaría-Pérez, D. Errandonea, E. Pérez-González, J. López-Solano, P. Rodríguez-Hernández, A. Muñoz, I. M. Tiginyanuf, and V. V. Ursaki, Mat. Res. Bull. **48**, 2128 (2013).

[42] D. Errandonea, J. Pellicer-Porres, F. J. Manjón, A. Segura, Ch. Ferrer-Roca, R. S. Kumar, O. Tschauner, J. López-Solano, P. Rodríguez-Hernández, S. Radescu, A. Mujica, A. Muñoz, and G. Aquilanti, Phys. Rev. B **73**, 224103 (2006).

[43] J. López-Solano, P. Rodríguez-Hernández, S. Radescu, A. Mujica, A. Muñoz, D. Errandonea, F. J. Manjón, J. Pellicer-Porres, N. Garro, A. Segura, Ch. Ferrer-Roca, R. S. Kumar, O. Tschauner, and G. Aquilanti, Physica Status Solidi (b) **244**, 325 (2007).

[44] F. J. Manjón, D. Errandonea, J. López-Solano, P. Rodríguez-Hernández, S. Radescu, A. Mujica, A. Muñoz, N. Garro, J. Pellicer-Porres, A. Segura, Ch. Ferrer-Roca, R. S. Kumar, O. Tschauner, and G. Aquilanti, Physica Status Solidi (b) **244**, 295 (2007).

[45] J. López-Solano, P. Rodríguez-Hernández, A. Muñoz, and F. J. Manjón, Phys. Rev. B **73**, 094117 (2006).